PERGAMON

International Journal of Solids and Structures 39 (2002) 4133–4149

INTERNATIONAL JOURNAL OF SOLIDS and STRUCTURES

www.elsevier.com/locate/ijsolstr

Ultrasonic waves in layered anisotropic media: characterization of multidirectional composites

S.I. Rokhlin *, L. Wang

Nondestructive Evaluation Program, Edison Joining Technology Center, The Ohio State University, 1248 Arthur E. Adams Drive, Columbus, OH 43221, USA

Received 27 January 2002; received in revised form 19 February 2002

Abstract

An efficient and stable recursive compliance/stiffness matrix algorithm is presented to model wave propagation in multidirectional composites. The models are applied to clarify angle beam transmission through a multidirectional composite and to process ultrasonic data for determination of the elastic properties of a composite lamina (single ply) from measurements on a multidirectional composite. Ultrasonic characterization of composites using double-through-transmission and time-resolved line focus acoustic microscopy has been addressed. The double-through-transmission measurements and simulations show that the transmission amplitude is highly dependent on ply orientation and angle of incidence. The transmission amplitude decreases rapidly with incident angle deviation from the normal; however, a transmission window is found in the incident angle range 45–60° at frequencies below 2.25 MHz. The time-delay measurements by the double-through-transmission technique have been used to reconstruct lamina properties using the Floquet wave concept. A unidirectional lamina elastic properties measurement using line focus acoustic microscopy of a multidirectional composite sample is also briefly discussed. The effective elastic properties for the composites are determined from the lamina properties by a Floquet wave dynamic homogenization method.

Keywords: Multidirectional composites; Wave propagation; Floquet waves; Stiffness matrix

1. Introduction

Ultrasonic characterization of composites has been an active field of study for the last several decades. The foundation for wave propagation in composites was laid in the early work of Achenbach et al. (1968) and Achenbach (1974). Several approximate and exact models have been developed since then for wave propagation in multidirectional composites; many of these have been reported in the proceedings edited by Mal and Ting (1988) and reviewed by Datta (2000). Approximate solutions include the effective media

* Corresponding author. Tel.: +1-614-292-7823; fax: +1-614-292-3395/6842.
E-mail address: rokhlin.2@osu.edu (S.I. Rokhlin).

0020-7683/02/$ - see front matter
PII: S0020-7683(02)00363-3

methods of Postma (1955) and Schoenberg and Muir (1989), the effective stiffness method of Sun et al. (1968) and Achenbach et al. (1968) and the thin layer method of Shah and Datta (1982) and Kausel (1986). Among the exact solutions the most widely used are the transfer matrix and global matrix methods. A transfer matrix method was developed by Adler and coworkers for a layered anisotropic medium using the exponential Stroh representation (Fahmy and Adler, 1973; Adler, 1990). The transfer matrix method in standard form was developed for general anisotropy by Nayfeh (1991, 1995). Experimental and theoretical examples for multidirectional composites are given by Chimenti and Nayfeh (1990) and Nayfeh and Chimenti (1991). To overcome the computational instabilities of the transfer matrix method, Castaings and Hosten (1993) and Hosten and Castaings (1993) generalized the delta matrix method to multilayered media with monoclinic layers (orthotropic layers arbitrarily rotated about one symmetry axis). Mal (1988) developed a computationally stable global matrix method for layered anisotropic media. A modified global matrix method using a layer stiffness matrix has been obtained for isotropic media by Kausel and Roesset (1981), for an orthotropic layer in the plane of symmetry by Wang and Rajapakse (1994) and by Wang et al. (1998), Wang and Rokhlin (2000) for generally anisotropic media. The global stiffness matrix method reduces by half the dimension of the global system of equations. Another stable approach is a generalization by Fryer and Frazer (1984, 1987) of the reflectivity method of Kennett and Kerry (1979) and Kennett (1983) to layered anisotropic media. The reflection/transmission matrices for a generally anisotropic layer between anisotropic solids have also been obtained by Rokhlin and Huang (1992) by a method similar to that of Kennett and Kerry. A large number of experimental methods applicable to composite characterization have been reviewed by Chimenti (1997).

Multidirectional composites are highly anisotropic multilayered structures, which significantly complicates the wave spectrum in both frequency and angle domains. Due to this complexity, the measurement of properties of multidirectional composites becomes complicated. One method of measuring the elastic constants is to use low frequency ultrasonic waves. In this case, the nonhomogeneous composite may be considered as an effective homogeneous medium. Therefore one can use the same procedures developed for a homogeneous layer to reconstruct the effective elastic constants from the wave velocity measurements. Examples of this have been given by Rose et al. (1987); Hosten (1992) and Lobkis et al. (2000). Chu and Rokhlin (1994) have proposed a method to determine lamina elastic moduli for [0/90] metal matrix composites without the effective media approach. However they neglected the effect of wave interference within a single lamina in the laminate on the time-delay measurements. Such an assumption is valid only for composites with thick laminas or for composites with small impedance mismatch between 90° and 0° laminas.

Line focus acoustic microscopy can also be applied to composite characterization. Achenbach with his students pioneered the development of line focus acoustic microscopy for characterization of multilayered thin film structures. Lee et al. (1994) measured elastic constants by directly fitting the experimental $V(z)$ curve with an acoustic microscopy model using continuous wave mode acoustic microscopy and later Li and Achenbach (1996, 1997) used time-resolved acoustic microscopy (see also Guo et al., 2000). Xiang et al. (1996) also studied time-resolved acoustic microscopy and applied it to homogeneous anisotropic material property measurement and Wang et al. (1998) have applied it to composites.

In this paper we review our recent modeling and experimental studies of the ultrasonic characterization of multidirectional composites. In Section 2 we describe a computationally stable recursive stiffness matrix method, recently developed by us, for wave propagation in layered generally anisotropic media. In Section 3, ultrasonic wave interaction with fluid-loaded multidirectional composites is discussed. Both modeling and experimental results are presented for oblique ultrasonic through transmission. Floquet wave spectra in angle and frequency domains are used for interpretation of the results. In Section 4, measurements of lamina elastic properties using Floquet waves and line focus time-resolved acoustic microscopy are described.

2. Ultrasonic model for multidirectional composites: Recursive stiffness/compliance matrix method

2.1. Lamina compliance/stiffness matrix

Let us consider a multilayered medium, consisting of N arbitrarily anisotropic layers between solid or liquid semi-spaces as illustrated in Fig. 1. In the jth layer, the displacement vector $\mathbf{u}_j$ may be written as the summation of six partial waves

$$\mathbf{u}_j = \sum_{n=1}^{3} (a_n^+ \mathbf{p}_n^+ \, e^{ik_z^{+n}(z-z_j)} + a_n^- \mathbf{p}_n^- \, e^{ik_z^{-n}(z-z_{j-1})})_j \, e^{i(k_x x + k_y y - \omega t)}, \tag{1}$$

where $\mathbf{u}_j = (u_x^j, u_y^j, u_z^j)^T$, (T represents transpose); n $(= 1, 2, 3)$ denotes nth partial wave; the superscripts $+$ and $-$ indicate wave propagation in $+z$- or $-z$-directions respectively; $\mathbf{p}_n^+$ and $\mathbf{p}_n^-$ $(\mathbf{p}_n^\pm = (p_x^\pm, p_y^\pm, p_z^\pm)_n^T)$ are the unit wave displacement polarization vectors corresponding to k_z^{+n} and k_z^{-n} wave numbers respectively. For each layer, we select the local coordinate origin at the top of the jth layer $(z = z_{j-1})$ for waves propagating along the $-z$-direction (a^-) and at the bottom of the jth layer $(z = z_j)$ for waves propagating along the $+z$-direction (a^+). Such a selection of the local coordinate system is very important for eliminating the numerical overflow of the exponential terms in Eq. (1) when the waves become nonhomogeneous (Schmidt and Tango, 1986; Schmidt and Jensen, 1985). The displacement polarization vectors $\mathbf{p}_n^\pm$ and wave numbers $k_z^{\pm n}$ are determined by solving the Christoffel equation (Rokhlin et al., 1986).

From Eq. (1), the displacement vector on the upper $(z = z_{j-1})$ $\mathbf{u}_{j-1}$ and lower surfaces $(z = z_j)$ $\mathbf{u}_j$ of the layer j can be represented in the matrix form

$$\begin{bmatrix} \mathbf{u}_{j-1} \\ \mathbf{u}_j \end{bmatrix} = \begin{bmatrix} \mathbf{P}^- & \mathbf{P}^+\mathbf{H}^+ \\ \mathbf{P}^-\mathbf{H}^- & \mathbf{P}^+ \end{bmatrix}_j \begin{bmatrix} \mathbf{A}_j^- \\ \mathbf{A}_j^+ \end{bmatrix}, \tag{2}$$

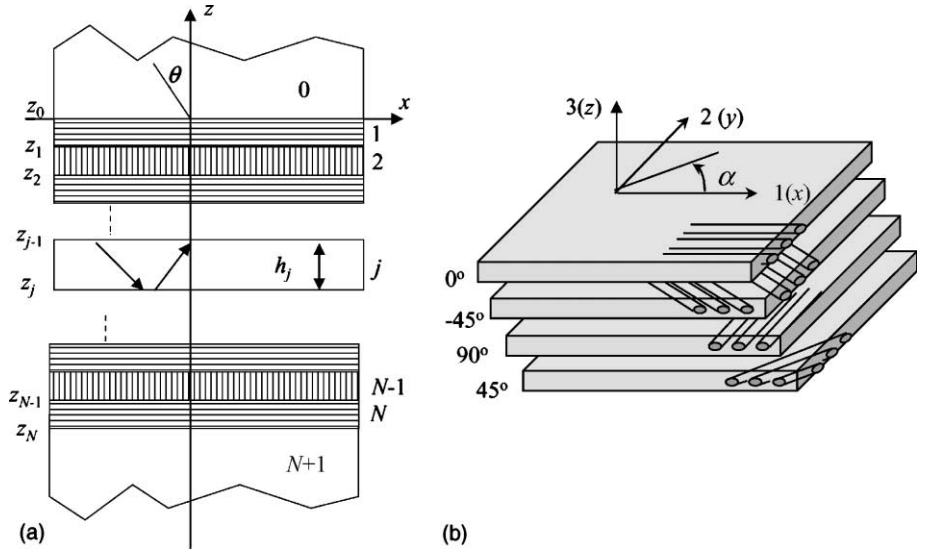

Fig. 1. (a) A multilayered structure and (b) composite cell formed by the lay-up of the unidirectional lamina (ply) and the reference coordinate system. The ultrasonic incident plane is oriented at angle α with relation to x-direction (fiber direction in the top lamina).

where

$$\mathbf{P}^{\pm}(3\times 3)=\left[\mathbf{p}_1^{\pm},\quad \mathbf{p}_2^{\pm},\quad \mathbf{p}_3^{\pm}\right],\qquad \mathbf{A}_j^{\pm}=\left[a_1^{\pm},\quad a_2^{\pm},\quad a_3^{\pm}\right]^{\mathrm{T}}$$

and

$$\mathbf{H}^{+}(3\times 3)=\mathrm{Diag}\left[\mathrm{e}^{\mathrm{i}k_z^{+1}h_j},\quad \mathrm{e}^{\mathrm{i}k_z^{+2}h_j},\quad \mathrm{e}^{\mathrm{i}k_z^{+3}h_j}\right],\qquad \mathbf{H}^{-}(3\times 3)=\mathrm{Diag}\left[\mathrm{e}^{-\mathrm{i}k_z^{-1}h_j},\quad \mathrm{e}^{-\mathrm{i}k_z^{-2}h_j},\quad \mathrm{e}^{-\mathrm{i}k_z^{-3}h_j}\right],$$

$h_j=z_{j-1}-z_j$ being the thickness of the jth lamina. If the z-axis is a symmetry axis, we have $k_z^{-n}=-k_z^{+n}$, therefore, $\mathbf{H}^{+}=\mathbf{H}^{-}$. This will be the case of monoclinic symmetry corresponding to arbitrary rotation of the orthotropic layer around the symmetry axis z. Using Hooke's law, the stresses on the top $\boldsymbol{\sigma}_{j-1}$ ($z=z_{j-1}$) and bottom surfaces $\boldsymbol{\sigma}_j$ ($z=z_j$) of the jth layer are related to the wave amplitudes $\mathbf{A}_j^{\pm}$ in the matrix form as

$$\begin{bmatrix}\boldsymbol{\sigma}_{j-1}\\ \boldsymbol{\sigma}_j\end{bmatrix}=\begin{bmatrix}\mathbf{D}^{-} & \mathbf{D}^{+}\mathbf{H}^{+}\\ \mathbf{D}^{-}\mathbf{H}^{-} & \mathbf{D}^{+}\end{bmatrix}\begin{bmatrix}\mathbf{A}_j^{-}\\ \mathbf{A}_j^{+}\end{bmatrix},\tag{3}$$

where $\mathbf{D}^{\pm}=[\mathbf{d}_1^{\pm},\quad \mathbf{d}_2^{\pm},\quad \mathbf{d}_3^{\pm}]$, the components $(d_i^{\pm})_j$ of vector $\mathbf{d}_j^{\pm}$ are related to the polarization vector $\mathbf{p}_j^{\pm}$ by $(d_i^{\pm})_j=(c_{i3ln}k_n p_l^{\pm})_j$, c_{ijln} represents the layer elastic constants.

Substituting into Eq. (2) the amplitude vectors $\mathbf{A}_j^{\mp}$ from Eq. (3), we obtain the layer stiffness $\mathbf{K}_j$ or compliance $\mathbf{S}_j$ matrices which relates the stresses to displacements at the layer top and bottom

$$\begin{bmatrix}\boldsymbol{\sigma}_{j-1}\\ \boldsymbol{\sigma}_j\end{bmatrix}=\begin{bmatrix}\mathbf{D}^{-} & \mathbf{D}^{+}\mathbf{H}\\ \mathbf{D}^{-}\mathbf{H} & \mathbf{D}^{+}\end{bmatrix}_j\begin{bmatrix}\mathbf{P}^{-} & \mathbf{P}^{+}\mathbf{H}\\ \mathbf{P}^{-}\mathbf{H} & \mathbf{P}^{+}\end{bmatrix}_j^{-1}\begin{bmatrix}\mathbf{u}_{j-1}\\ \mathbf{u}_j\end{bmatrix}=\mathbf{K}_j\begin{bmatrix}\mathbf{u}_{j-1}\\ \mathbf{u}_j\end{bmatrix},$$

$$\begin{bmatrix}\mathbf{u}_{j-1}\\ \mathbf{u}_j\end{bmatrix}=\begin{bmatrix}\mathbf{P}^{-} & \mathbf{P}^{+}\mathbf{H}\\ \mathbf{P}^{-}\mathbf{H} & \mathbf{P}^{+}\end{bmatrix}_j\begin{bmatrix}\mathbf{D}^{-} & \mathbf{D}^{+}\mathbf{H}\\ \mathbf{D}^{-}\mathbf{H} & \mathbf{D}^{+}\end{bmatrix}_j^{-1}\begin{bmatrix}\boldsymbol{\sigma}_{j-1}\\ \boldsymbol{\sigma}_j\end{bmatrix}=\mathbf{S}_j\begin{bmatrix}\boldsymbol{\sigma}_{j-1}\\ \boldsymbol{\sigma}_j\end{bmatrix},\tag{4}$$

where $\mathbf{S}_j=\mathbf{K}_j^{-1}$.

As we will see below, it is convenient to consider both stiffness and compliance matrices, and depending on the application, one or another formulation will be used.

It is convenient to subdivide the stiffness/compliance matrix $M(6\times 6)$ into four 3×3 submatrices $\mathbf{M}_{11}$, $\mathbf{M}_{12}$, $\mathbf{M}_{21}$, $\mathbf{M}_{22}$; here $\mathbf{M}$ is the $\mathbf{S}$ or $\mathbf{K}$ matrix. When the x–y (1–2) plane is a symmetry plane of the lamina, which is the case for laminated composites, the stiffness/compliance matrix has some symmetry:

$$\begin{aligned}\mathbf{M}_{11}&=\begin{bmatrix}M_{11} & M_{12} & M_{13}\\ M_{12} & M_{22} & M_{23}\\ -M_{13} & -M_{23} & M_{33}\end{bmatrix},\qquad \mathbf{M}_{12}=\begin{bmatrix}M_{14} & M_{15} & M_{16}\\ M_{16} & M_{25} & M_{26}\\ M_{16} & M_{26} & M_{36}\end{bmatrix},\\ \mathbf{M}_{22}&=\begin{bmatrix}-M_{11} & -M_{12} & M_{13}\\ -M_{12} & -M_{22} & M_{23}\\ -M_{13} & -M_{23} & -M_{33}\end{bmatrix},\qquad \mathbf{M}_{21}=\begin{bmatrix}-M_{14} & -M_{15} & M_{16}\\ -M_{16} & -M_{25} & M_{26}\\ M_{16} & M_{26} & -M_{36}\end{bmatrix}.\end{aligned}\tag{5}$$

Due to the symmetry only 12 elements M_{ij} of the matrix $\mathbf{M}$ are independent.

2.2. Recursive algorithm to obtain the total compliance/stiffness matrix

To obtain the global compliance/stiffness matrix for a multilayered structure, we have developed a recursive algorithm based on the compliance/stiffness matrix for a single layer. The recursive procedure is

$$\mathbf{M}^{J}=\begin{bmatrix}\mathbf{M}_{11}^{J-1}+\mathbf{M}_{12}^{J-1}(\mathbf{M}_{11}^{j}-\mathbf{M}_{22}^{J-1})^{-1}\mathbf{M}_{21}^{J-1} & -\mathbf{M}_{12}^{J-1}(\mathbf{M}_{11}^{j}-\mathbf{M}_{22}^{J-1})^{-1}\mathbf{M}_{12}^{j}\\ \mathbf{M}_{21}^{j}(\mathbf{M}_{11}^{j}-\mathbf{M}_{22}^{J-1})^{-1}\mathbf{M}_{21}^{J-1} & \mathbf{M}_{22}^{j}-\mathbf{M}_{21}^{j}(\mathbf{M}_{11}^{j}-\mathbf{M}_{22}^{J-1})^{-1}\mathbf{M}_{12}^{j}\end{bmatrix},\tag{6}$$

where $\mathbf{M}^J$ is the total compliance $\mathbf{S}^J$ or stiffness $\mathbf{K}^J$ matrix for the top J layers, $\mathbf{M}_{mn}^{J-1}$ are the total compliance/stiffness submatrices for the top $J-1$ layers, $\mathbf{M}_{mn}^{j}$ are the compliance/stiffness submatrices for the jth layer. As has been shown by Wang and Rokhlin (2001), the compliance/stiffness matrix formulation (4) and the recursive algorithm (6) are computationally stable in an arbitrary frequency range and have the computational efficiency of the transfer matrix method. Note that in Eq. (6), the submatrix $\mathbf{M}_{22}^J$ of the total compliance/stiffness matrix $\mathbf{M}^J$ for the top m layers depends only on submatrix $\mathbf{M}_{22}^{J-1}$ of the total compliance/stiffness matrix $\mathbf{M}^{J-1}$ for the top $j-1$ layers and compliance/stiffness submatrices for the layer j. Therefore $\mathbf{M}_{22}^J$ can be obtained recursively without calculating all other submatrices of the total compliance/stiffness matrix. This is useful when one needs only to calculate the total compliance/stiffness matrix $\mathbf{M}_S^J$ for a layered half space ($\mathbf{M}_S^J = \mathbf{M}_{22}^J$).

2.3. Application to composites with periodicity and symmetry

For materials with structural periodicity, which is the case for most composites, the recursive method allows very efficient computation of the total stiffness matrix. Let us introduce a repetitive cell consisting of n different anisotropic layers; we define it as $[\theta_1/\theta_2/\cdots/\theta_{n-1}/\theta_n]_{ps}$. Here θ_i indicates a layer in the cell p with the ply orientation angle θ_i. For example, [0°/45°/90°/−45°] represents a four layered cell ($n = 4$) (Fig. 1b) obtained by a combination of 0°, 45°, 90° and −45° unidirectional laminas (plies). The index p indicates the number of cells in the layered structure without symmetry or half of the layers for the system with symmetry; the index s indicates the structure symmetry. Using the recursive algorithm (Eq. (6)), one first calculates the compliance/stiffness matrix of the layered cell. The global compliance/stiffness matrix is calculated accounting for the repetition of the cells by application of Eq. (6) to the cell compliance/stiffness matrix. If $p = 2^i$ then only i recursive operations are required to obtain the total compliance/stiffness with p repetitive cells. If the structure is symmetric about its center line, the global stiffness/compliance matrix of a symmetrical composite holds symmetry properties (5); and the total compliance/stiffness matrices $\mathbf{M}^{\mathrm{B}}(\mathbf{M}_{ij}^{\mathrm{B}})$ of the bottom half of the structure is related to that of the top half structure $\mathbf{M}^{\mathrm{T}}(\mathbf{M}_{ij}^{\mathrm{T}})$ as

$$\mathbf{M}_{ij}^{\mathrm{B}} = -\mathbf{I}_2\mathbf{M}_{(3-i)(3-j)}^{\mathrm{T}}\mathbf{I}_2, \quad (i,j=1,2), \tag{7}$$

where

$$\mathbf{I}_2 = \begin{bmatrix} 1 & 0 & 0 \\ 0 & 1 & 0 \\ 0 & 0 & -1 \end{bmatrix}.$$

Therefore, once the compliance/stiffness matrix for the top half structure $[\theta_1/\theta_2/\cdots/\theta_{n-1}/\theta_n]_p$ has been calculated, the stiffness matrix for the bottom half can be immediately determined by Eq. (7) and the total stiffness matrix for the whole structure $[\theta_1/\theta_2/\cdots/\theta_{n-1}/\theta_n]_{ps}$ is obtained by combining them using Eq. (6).

2.4. Infinite periodic media

For further discussion of the lamina property measurements we need to formulate the Floquet wave characteristic equation for propagation in a periodic anisotropic medium. The Floquet theory requires periodicity conditions (Nayfeh, 1991; Braga and Herrmann, 1992) on the unit cell surface:

$$\begin{bmatrix} \mathbf{u}^+ \\ \boldsymbol{\sigma}^+ \end{bmatrix} = \mathrm{e}^{\mathrm{i}\zeta h_c}\begin{bmatrix} \mathbf{u}^- \\ \boldsymbol{\sigma}^- \end{bmatrix}, \tag{8}$$

where ζ represents the Floquet wave number and h_c the thickness of the unit cell. The cell stiffness matrix $\mathbf{K}_{\mathrm{c}}$ for a periodic medium is obtained using the recursive algorithm. It relates the stresses and displacements on the top $(\boldsymbol{\sigma}^+, \mathbf{u}^+)$ and bottom $(\boldsymbol{\sigma}^-, \mathbf{u}^-)$ surfaces of the cell:

$$\begin{bmatrix} \boldsymbol{\sigma}^+ \\ \boldsymbol{\sigma}^- \end{bmatrix} = \begin{bmatrix} \mathbf{K}_c^{11} & \mathbf{K}_c^{12} \\ \mathbf{K}_c^{21} & \mathbf{K}_c^{22} \end{bmatrix} \begin{bmatrix} \mathbf{u}^+ \\ \mathbf{u}^- \end{bmatrix}. \tag{9}$$

Using the cell stiffness matrix (Eq. (9)) and periodicity condition (8), we obtain the equivalent of the Christoffel equation for Floquet waves:

$$(e^{i\zeta h_c}\mathbf{K}_c^{21} - e^{-i\zeta h_c}\mathbf{K}_c^{12} + \mathbf{K}_c^{22} - \mathbf{K}_c^{11})\mathbf{u}^- = 0, \tag{10}$$

$\mathbf{u}^-$ is the Floquet wave unit displacement vector and is equivalent to the displacement polarization $\mathbf{p}$. The characteristic equation of the Floquet wave for arbitrarily anisotropic media is obtained by equating the determinant of the system (10) to zero.

2.5. Point source response: Green's function for multiply composites

To describe in layered elastic systems an impulse dynamic effect such as acoustic emission (Lih and Mal, 1996; Green and Green, 2000a,b) or laser generation of ultrasound (Cheng et al., 2001) one needs a solution for point sources. The point source response is also essential for solving the scattering problem using the boundary element method. Below we apply the recursive stiffness matrix method to derive the Green's function for a layered anisotropic medium. For the source description we employ the method of Kennett (1983) and Fryer and Frazer (1984) who showed that a dislocation source can be represented by discontinuities in displacements and tractions across the source plane $z = z_s$:

$$\hat{\mathbf{u}}(z_s^+) - \hat{\mathbf{u}}(z_s^-) = \boldsymbol{\Delta}_u; \qquad \hat{\boldsymbol{\sigma}}(z_s^+) - \hat{\boldsymbol{\sigma}}(z_s^-) = \boldsymbol{\Delta}_\sigma, \tag{11}$$

where the symbol '$\wedge$' denotes the wave number domain. The relation of the displacement $\boldsymbol{\Delta}_u$ and traction $\boldsymbol{\Delta}_\sigma$ jumps to the source tensor is given by Kennett (1983).

The solution is obtained in two steps: (1) Using boundary and radiation conditions on the layered system top $z = z_0$ and bottom $z = z_N$ planes (Fig. 1) the stresses and displacements in the plane of the sources $z = z_s$ are found in terms of the source discontinuities. (2) Using stresses and displacements at the source plane, the stresses and displacements in other planes are calculated using the two stiffness/compliance matrices relating the stresses and displacements at this interface and those at the top and source planes.

Step 1: Displacements and stresses in the source plane: The compliance matrix $\mathbf{S}^U$ between planes z_0 and z_s^+ and the compliance matrix $\mathbf{S}^B$ between planes z_s^- and z_N are calculated recursively using the respective layer compliance matrices. They relate the displacements and stresses at the source plane to those at the top and bottom surfaces of the layered system

$$\begin{bmatrix} \hat{\mathbf{u}}(z_0) \\ \hat{\mathbf{u}}(z_s^+) \end{bmatrix} = \begin{bmatrix} \mathbf{S}_{11}^U & \mathbf{S}_{12}^U \\ \mathbf{S}_{21}^U & \mathbf{S}_{22}^U \end{bmatrix} \begin{bmatrix} \hat{\boldsymbol{\sigma}}(z_0) \\ \hat{\boldsymbol{\sigma}}(z_s^+) \end{bmatrix}, \qquad \begin{bmatrix} \hat{\mathbf{u}}(z_s^-) \\ \hat{\mathbf{u}}(z_N) \end{bmatrix} = \begin{bmatrix} \mathbf{S}_{11}^B & \mathbf{S}_{12}^B \\ \mathbf{S}_{21}^B & \mathbf{S}_{22}^B \end{bmatrix} \begin{bmatrix} \hat{\boldsymbol{\sigma}}(z_s^-) \\ \hat{\boldsymbol{\sigma}}(z_N) \end{bmatrix}. \tag{12}$$

Assuming the layered structure has free top and bottom surfaces ($\hat{\boldsymbol{\sigma}}(z_0) = \hat{\boldsymbol{\sigma}}(z_N) = 0$). We have from Eq. (12):

$$\hat{\mathbf{u}}(z_s^+) = \mathbf{S}_{22}^U \hat{\boldsymbol{\sigma}}(z_s^+), \quad \hat{\mathbf{u}}(z_s^-) = \mathbf{S}_{11}^B \hat{\boldsymbol{\sigma}}(z_s^-). \tag{13}$$

Substituting Eq. (13) into Eq. (11), one obtains the displacements at z_s^+ as functions of the source strength terms Δ_u and Δ_σ:

$$\hat{\mathbf{u}}(z_s^+) = (\mathbf{I} - \mathbf{S}_{11}^B(\mathbf{S}_{22}^U)^{-1})^{-1}(\Delta_u - \mathbf{S}_{11}^B \Delta_\sigma). \tag{14}$$

Other displacements and stresses $\hat{\mathbf{u}}(z_s^-)$, $\hat{\boldsymbol{\sigma}}(z_s^\pm)$, $\hat{\mathbf{u}}(z_0)$ and $\hat{\mathbf{u}}(z_N)$ at the source plane and at the top and bottom surfaces of the structure are obtained from Eqs. (12) and (13).

Step 2: Displacements and stresses at the receiver planes: For stable computation of the field in the receiver planes $z = z_r$ inside the structure, which is the case of embedded sensors, one should utilize the "back propagation" recursive algorithm (Wang and Rokhlin, 2002a; Rokhlin and Wang, 2002). These displacements and stresses are recursively determined from the known displacement $\hat{\mathbf{u}}(z_s^{\pm})$, $\hat{\mathbf{u}}(z_0)$ and $\hat{\mathbf{u}}(z_N)$ and stresses $\hat{\boldsymbol{\sigma}}(z_s^{\pm})$ using the two stiffness/compliance matrices between the receiver interface $z = z_r$ and the system top surface z_0 and the source interface z_s.

The displacement $\mathbf{u}(x, y, z, t)$ and stress $\boldsymbol{\sigma}(x, y, z, t)$ in time and spatial domains are obtained by the inverse Fourier transform.

$$\mathbf{u}(x, y, z, t) = \int_{-\infty}^{+\infty} e^{i\omega t}\, d\omega \int_{-\infty}^{+\infty} \hat{\mathbf{u}}(k_x, k_y, \omega)\, e^{i(k_x x + k_y x)} dk_x dk_y. \tag{15}$$

3. Ultrasonic wave interaction with fluid-loaded multidirectional composites

3.1. Reflection and transmission coefficients

For ultrasonic evaluation of composites, they are usually immersed in fluid and inspected in reflection or through transmission mode. Thus it is important to understand the ultrasonic wave reflection and through transmission for this and many other ultrasonic applications. Let us consider a plane acoustic wave incident from fluid onto an anisotropic layered structure immersed in the fluid. Using the total compliance matrix for the structure and the boundary conditions on the fluid–solid interfaces we obtain for the transmission T and the reflection R coefficients for laminates immersed in fluid (Wang and Rokhlin, 2001)

$$T = 2\Lambda S_{21}^{33} / [(S_{11}^{33} + \Lambda)(S_{22}^{33} - \Lambda) - S_{21}^{33} S_{12}^{33}], \tag{16}$$

$$R = [(S_{11}^{33} - \Lambda)(S_{22}^{33} - \Lambda) - S_{21}^{33} S_{12}^{33}] / [(S_{11}^{33} + \Lambda)(S_{22}^{33} - \Lambda) - S_{21}^{33} S_{12}^{33}], \tag{17}$$

where the S_{ij}^{33} are the (3,3) elements in the submatrices $\mathbf{S}_{ij}(3 \times 3)$ of the total (6×6) compliance matrix $\mathbf{S}$ for the composite structure and $\Lambda = \cos\theta / (i\omega\rho_f V_f)$, ρ_f is the fluid density, and V_f is the acoustic velocity in the fluid, θ is the incident angle.

3.2. Modal solution

The guided wave characteristic equation for a layered anisotropic medium is obtained from the total stiffness matrix ($\mathbf{K}$) of the structure using the free boundary conditions at the top and bottom surfaces. The guided wave characteristic equation is given as

$$\det(\mathbf{K}) = 0. \tag{18}$$

For a fluid-loaded layered anisotropic structure, the dispersion equation for leaky Lamb modes can be determined from the reflection and transmission coefficients (Eqs. (16) and (17)), by equating the denominator to zero:

$$(S_{11}^{33} + \Lambda)(S_{22}^{33} - \Lambda) - S_{21}^{33} S_{12}^{33} = 0. \tag{19}$$

3.3. Angle beam through transmission: experiment and simulation

At oblique incidence of ultrasonic waves on a multidirectional composite, the reflection/transmission phenomena become very complicated (Rokhlin et al., 1999) due to the appearance of nontransmittance

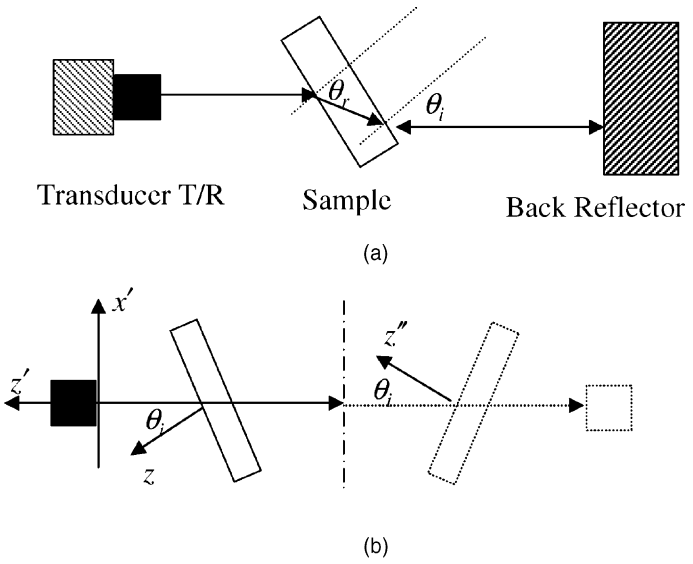

Fig. 2. (a) Schematic diagram of the self-reference bulk wave method and (b) equivalent representation of the measurement used for modeling. The dashed lines indicate the mirror reflection of the back propagation path. Mirror plane is indicated by the broken vertical line.

zones. In this section we will compare experimental and theoretical results for the double transmission ultrasonic measurements shown schematically in Fig. 2. The ultrasonic signal is transmitted through the multiply composite sample immersed in the fluid, then reflected from the plane reflector and returned to the transducer. The sample is rotated in two planes, thus angles of incidence and plane of incidence can be continuously changed.

The schematic diagram of the double-through-transmission method is given in Fig. 2. We consider the back reflector as a mirror with Fig. 2b showing the wave travel path used in the model. Accounting for the phase delay in fluid as shown in Fig. 2b, one can obtain the time-domain voltage output:

$$V_{\text{out}}(t) = \int_{-\infty}^{+\infty} F(\omega)\,\mathrm{d}\omega \int_{-\infty}^{+\infty} \Phi_{\text{t}}(k'_x) T_{\text{t}}(k_x) T_{\text{b}}(k''_x)\, \mathrm{e}^{\mathrm{i}(-2k'_z L + k_z \mathrm{d} + k''_z \mathrm{d})}\,\mathrm{d}k'_x, \tag{20}$$

where L is the distance between the surfaces of the transducer and back reflector, d is the thickness of the sample. $k_z = \sqrt{(\omega/V_{\text{f}})^2 - k_x^2}$, V_{f} is acoustic velocity in the fluid. k'_x, k'_z and k''_x, k''_z are the wave numbers in the coordinator systems rotated from the axis z (Fig. 2b) by θ_i (primed) and $2\theta_i$ (double primed) respectively (z' is the normal to the transducer face). $F(\omega)$ is the frequency response of the transmitter/receiver; $\Phi_{\text{t}}(k'_x)$ is the angular response of the transducer. They are experimentally determined by inverting the measured reflection signal from a homogeneous semi-space such as a block of aluminum. $T_{\text{t}}(k_x)$ and $T_{\text{b}}(k''_x)$ are the transmission coefficients through the layer for the wave incident from fluid on the layer top or bottom respectively.

Here we experimentally and theoretically investigate wave transmission through a $[0/45/90/-45]_{2\text{s}}$ composite whose lamina properties are given in Table 1. Fig. 3a shows the peak amplitude versus incident angle for the incident plane orientation $\alpha = 25°$ (Fig. 1b). Fig. 3b compares experimental (dots) and computed (solid lines) time domain signals for several incident angles. The incident wave signal has center frequency 2.25 MHz. At normal incidence (0°), the multiple reflections in the sample are clearly identified. At 14° incident angle, the transmitted signal reaches the first maximum and clearly shows dispersion and strong distortion. Above 14° the amplitude drops, reaching the noise level at 30°. The transmitted signal

Table 1
Lamina properties

Lamina elastic constants (GPa)								
C_{11}	C_{22}	C_{33}	C_{44}	C_{55}	C_{66}	C_{12}	C_{13}	C_{13}
143.2	15.8	15.8	3.8	7.0	7.0	7.5	7.5	8.2
Density (g/cm^3)	Lamina thickness (mm)							
1.6	0.194							

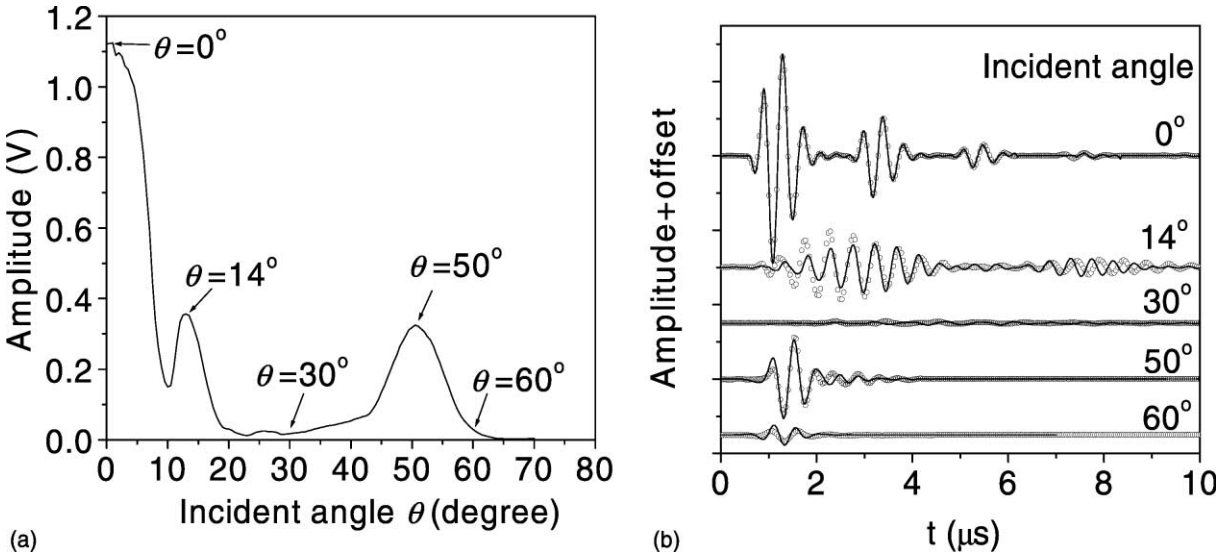

Fig. 3. (a) Measured peak amplitude of the first double through transmission signal versus incident angle θ and (b) measured (◯) and calculated (—) time domain signals for six typical incident angles. The incident plane orientation angle α is 22.5° and pulse center frequency is 2.25 MHz.

amplitude reaches an additional maximum at 50° whereas spectrum analysis shows the center transmitted frequency at about 2 MHz.

To further clarify the transmission properties of the composite, double through transmission measurements and computations are presented with steps of 1° in the range of orientation angles from 0° to 180° in image form (Fig. 4a). In these images, the radial direction represents the incident angle θ and the circumferential direction represents the orientation angle α. The gray level represents the amplitude; the brighter the gray level, the higher the transmitted amplitude. By comparing both calculated and measured data, one can conclude: (1) the double through transmission amplitude has 180° rotation symmetry; (2) it has no reflection symmetry (α and $-\alpha$); (3) at incident angles close to normal incidence (<7°) (marked by arrow L in Fig. 4), the multilayered composite is similar to an isotropic plate; (4) both experiment and calculation show a transmission peak at $10° < \theta < 20°$ and $-10° < \alpha < -75°$. The transmitted signals at this peak are strongly distorted (marked by arrow M); (5) a large transmission peak also appears in the incident angle range between 45° and 55°, where the energy is transmitted in the composite by the slow transverse wave. Within this range, the maximum transmission amplitude depends on rotation angle. Maximum values appear around rotation angles 22° and 60° (marked by arrow T in Fig. 4). The composite behaves as a low pass filter with a frequency band below 2 MHz.

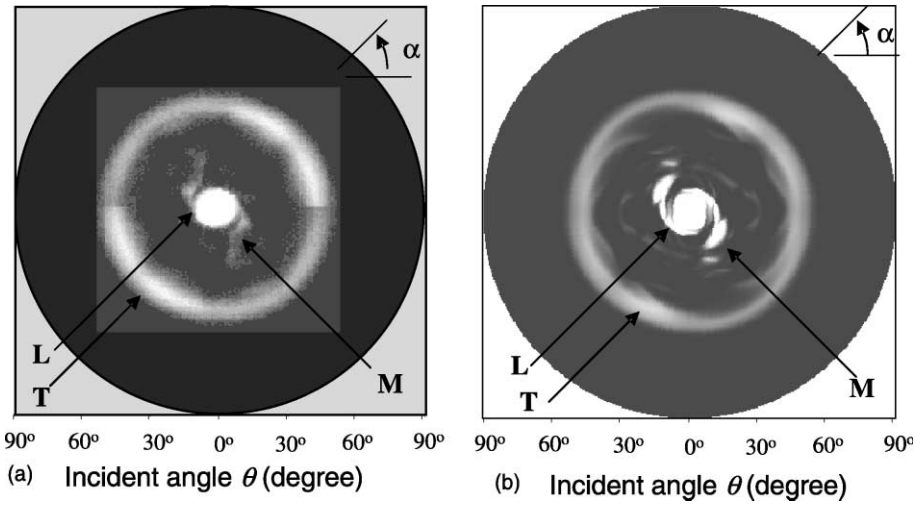

Fig. 4. The peak double through transmission amplitude for the $[0/45/90/-45]_{2s}$ composite as function of orientation α and incident θ angles. The transducer center frequency is 2.25 MHz. The gray level represents the transmission amplitude (while is maximum). (a) Experiment and (b) theory.

It is useful to apply the Floquet wave spectrum for a qualitative discussion of the phenomena observed in Fig. 4. Fig. 5a shows the stop and pass bands of the three Floquet waves as a function of composite orientation angle α and incident angle θ at frequency 2.25 MHz. The four gray levels represent the number of propagating Floquet waves (waves with real wave numbers). Black represents the stop band for all three

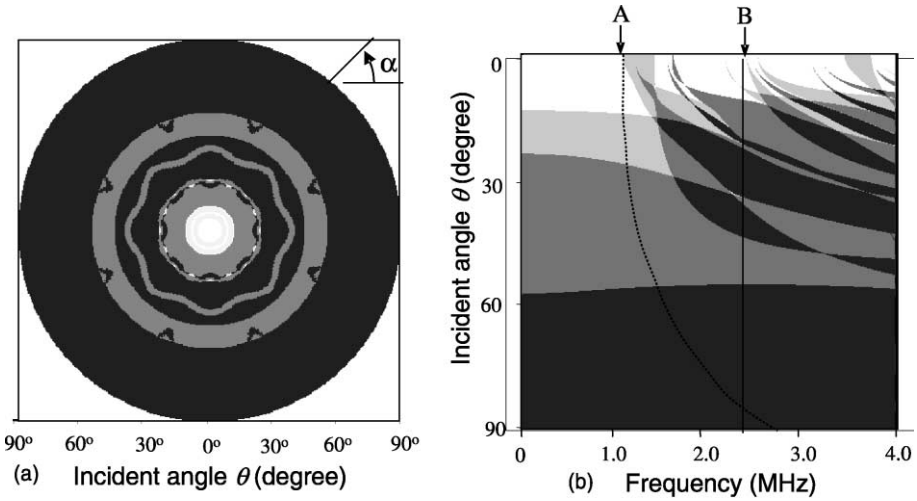

Fig. 5. Spectrum of pass and stop bands for the three Floquet waves for $[0/45/90/-45]_{2s}$ composite: (a) as a function of incident angle θ and incident plane orientation angle α, frequency is 2.25 MHz and (b) as a function of incident angle θ and frequency with the propagating plane oriented at $\alpha = 0°$. White domains correspond to all three propagating waves, light gray to two propagating waves and darker gray to one propagating wave, black corresponds to the stop band for all three waves (no propagating waves permitted). The frequency indicated by the arrow 'B' corresponds to the polar diagram shown in Fig. 5a. The dashed line indicated by the arrow 'A' corresponds to the approximate equation (22).

Floquet waves and white corresponds to the pass band domain for all three waves. As can be seen, all three Floquet waves have a pass band at incident angles below 10°. A pass band which is almost independent of orientation angle α appears for the slowest Floquet wave in the incident angle range 40–60°. Comparing this figure with the transmission amplitude distribution shown in Fig. 4a, one can see that the pass and stop bands of the Floquet waves determine the transmission amplitude distribution. Fig. 5b shows the Floquet wave stop and pass bands in the incident angle versus frequency domain. At frequencies below the first stop band, the multidirectional composites can be considered as a homogeneous medium (Wang and Rokhlin, 2000). At frequencies above the homogenization domain, a complicated spectrum of pass and stop bands exists. The stop and pass bands act as narrow band filters in both frequency and incident angle domains and lead to complicated time-domain signal distortion as shown in Fig. 3b at incident angle 14° or very small transmission at 30°. For higher incident angles, the homogenization domain is extended to the higher frequency range.

4. Elastic property measurements of composite lamina (ply)

Ultrasonic determination of the elastic properties of a single lamina from measurements on multiply composites has been a challenge to the nondestructive evaluation community. Here we will briefly discuss two methods to obtain the elastic properties of a unidirectional lamina from measurements on multidirectional composites: time-resolved acoustic microscopy and a Floquet-wave-based double-through-transmission method.

4.1. Lamina property measurements using time-resolved line focus acoustic microscopy

In line focus acoustic microscopy a cylindrically shaped line focus transducer is utilized. The coupling fluid between transducer and specimen is usually water. Models for line focus acoustic microscopy are well established (Briggs, 1992; Lee et al., 1994; Li and Achenbach, 1996, 1997). For line focus time-resolved acoustic microscopy, the response can be represented as

$$V_{\text{out}}(z,t) = \int_{-\infty}^{+\infty} F(\omega) \mathrm{e}^{\mathrm{i}\omega t}\,\mathrm{d}\omega \int_0^{\theta_M} P(\theta) R(\theta,\omega)\,\mathrm{e}^{2\mathrm{i}(\omega/V_{\mathrm{f}})d_0\cos\theta}\,\mathrm{d}\theta, \tag{21}$$

where $F(\omega)$ is the frequency and $P(\theta)$ is the pupil function of the transducer in the pulse echo mode, θ_M is the semi-aperture angle of the acoustic lens and d_0 is the defocus distance. $R(\theta,\omega)$ is the reflection coefficient from the sample, V_{f} is the acoustic velocity in the fluid.

Our experiments were performed with the line focus transducer, developed at NIST, which has center frequency 6 MHz, focus length 24.5 mm and half aperture angle 32°. Figs. 6 and 7 show the acoustic microscopy response for a unidirectional and a quasi-isotropic composite ($[45/0/-45/90]_{2s}$) respectively for different lens orientation with relation to the fiber direction in the top lamina. In these figures solid lines are experiment and dotted lines are theory. For a unidirectional composite as shown in Fig. 6, the signals in the response can be put in three categories: (1) normal specular reflections which correspond to normal incident rays (L_1 and L_2); (2) lateral waves which correspond to rays incident at critical angles (L_{a}); (3) bulk wave reflections which correspond to rays mode-converted and reflected from the bottom surface (LS_2, S_1S_1, S_1S_2; L denotes longitudinal and S_1, S_2 denote fast and slow quasi-transverse waves). The time delays of the normal specular reflections (L_1 and L_2) are used to determine the elastic constant $C_{33}(= C_{22})$. These signals are not shifted in the time domain with rotation angle. The time delays and amplitudes of these lateral wave and bulk wave reflections are significantly dependent on the rotation angle. Because the half aperture angle of our transducer is 32°, only the longitudinal lateral wave (L_{a}) has been observed. The leaky surface wave

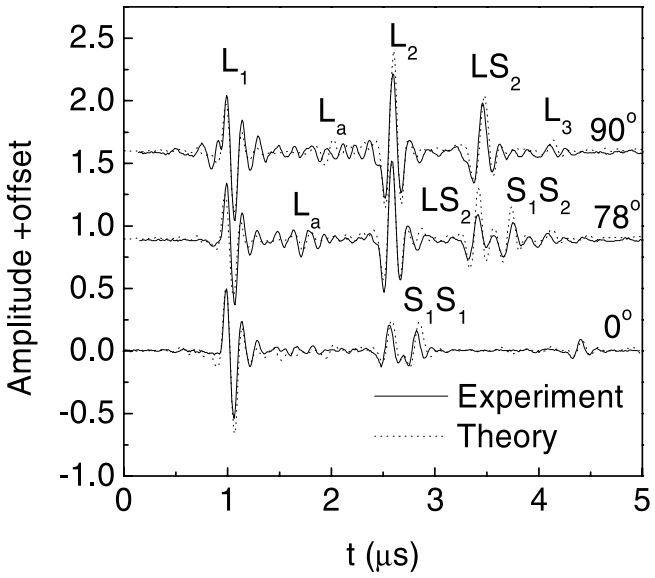

Fig. 6. Line focus microscopy signature at different rotation angles for the unidirectional composite plate with thickness 2.4 mm. The cylindrical transducer with PVDF film has center frequency 6 MHz and focus length 24.5 mm. Solid lines are experiment; doted lines are simulations.

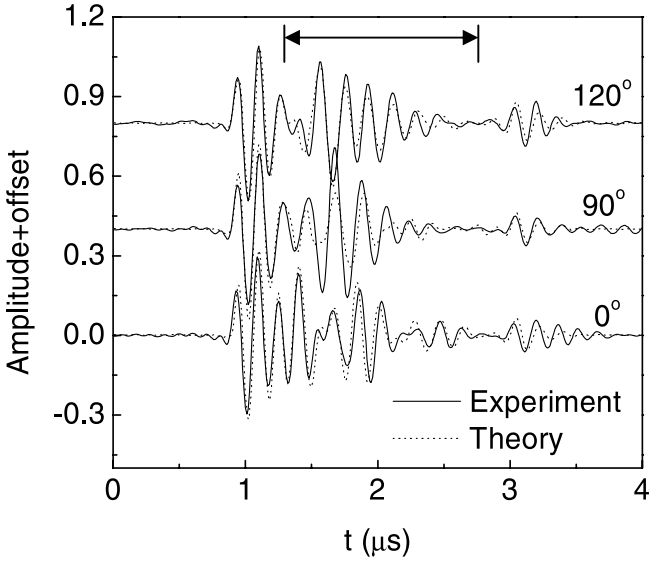

Fig. 7. Line focus microscopy signature for a multilayered $[45/0/-45/90]_{2s}$ composite at different angles of lens orientation. Solid lines are experiment and dotted lines are simulation.

does not exist in these materials since its speed increases above the transverse wave speed due to the fluid loading effect.

For the quasi-isotropic composite, the reflection signature becomes much more complicated; however, the model describes the experimental observations well. The oblique rays form a complex reflection sig-

nature due to interference of reflected signals from different interfaces at various incident angles. Therefore we cannot simply interpret these signals as bulk shear or longitudinal wave reflections.

The inverse reconstruction of the lamina elastic constants is performed from the measurements on the multidirectional composite in the time domain gate indicated in Fig. 7 (the specular surface reflection is excluded). The gated signatures for the set of rotation angles of the transducer are selected for further processing together with the computed signal gated at the same conditions. The lamina elastic constants are obtained by a least-squares minimization algorithm to match the computed and experimental signatures.

4.2. Floquet wave based lamina properties measurement

Due to the periodicity of the composite structure, the Floquet wave approach seems well suited for medium characterization. Floquet waves are formed in a periodic medium naturally accounting for the wave interference in the structure and their wave speed has a clear physical meaning. The Floquet wave theory provides a method to calculate the time delay for a signal propagating through a multiply composite and to determine the lamina elastic constants.

We already discussed in Section 3.3 the stop and pass bands of the Floquet wave spectrum shown in Fig. 5b in the k_x–ω domain. At frequencies above the first stop band, the Floquet wave velocity is very dispersive which leads to strong distortion of the transmitted signals. This leads to difficulties in time-delay measurement in this frequency range. At frequencies below the first stop band, the Floquet behavior is similar to that of a plane wave propagating in an anisotropic dispersive homogeneous medium. In this frequency domain, we may consider the periodic medium as an effective homogeneous anisotropic medium (Wang and Rokhlin, 2000, 2002b). We found that an approximate upper frequency f_h bound of the homogenization domain is given by

$$\frac{h_c}{\lambda_{\min}(\theta)}\cos\theta < 0.5, \tag{22}$$

where h_c is the cell thickness; $\lambda_{\min}$ and $V_{\min} = \omega/k_{\max}$ are the corresponding minimum wavelength and velocity at a given bulk wave propagation angle θ to the z-axis. The estimated homogenization domain using Eq. (22) for a [0/45/90/−45] composite is shown by the dashed curve in Fig. 5b.

We propose a method for lamina properties reconstruction based on application of the Floquet wave theory to processing of the data obtained by the self-reference double-through-transmission method. The difference between this method and the methods used for homogeneous anisotropic media (Rokhlin and Wang, 1992) is in how the time-delay calculation is done. For homogeneous media, the time delay is calculated using the phase velocity determined from the Christoffel equation. To calculate the time delay for a periodic medium we use the Floquet wave phase velocity obtained from Eq. (9). In this method, the time delays are measured for a set of incident angles in one or several orientations of the incident plane. Then the least-squares algorithm is applied to minimize the error between the experimental time delays and those calculated using the Floquet theory. The unknown lamina moduli of the composite are found by minimizing the sum of the squares of the deviations between the experimental and calculated time delays considering the elastic constants as variables in a multidimensional space (for details see Wang and Rokhlin, 2002c).

To check the stability and accuracy of the reconstruction, we performed computer simulations on a set of synthetic velocity data with random scatter, similar to the method described by Rokhlin and Wang (1992). The results are given in Table 2 for composite [0/45/90/−45]. First the time delay was calculated for selected orientations of the incident plane and a discrete set of refraction angles using the set of elastic constants of the lamina (given in the first row of the table). Next, random scatter was added to the time-delay data with data scatter levels 1% and 5%. The sets of time delays obtained serve as synthetic sets of experimental data. The initial guesses of the lamina elastic constants selected for reconstruction are given in

Table 2
Results of reconstruction from velocity data in the $\alpha = 0°$ incident plane of [0/45/90/−45] periodic composite

	C_{11}	C_{22}	C_{12}	C_{23}	C_{55}
Original value	143.2	15.8	7.5	8.2	7
Intial guess	214.8	12.8	3.75	4.1	10.5
No scatter	0%	0%	0%	0%	0%
1% scatter	0.04%	0.01%	0.7%	0.03%	0.03%
5% scatter	0.5%	0.04%	2.27%	1.03%	3.05%

the second row of the table. These values are at least 50% different from the exact values used for synthetic sets determination (given in the first row). Using this data with scatter, the lamina elastic constants are obtained using the reconstruction procedure discussed above. The relative error between the reconstructed elastic constants and the exact elastic constants are given in the third row (0% data scatter level), fourth row (1% data scatter level) and fifth row (5% data scatter level). One can see the lamina properties can be well recovered for "noise" time-delay data and initial guesses far from the exact value.

As an example the measurements were performed on a $[0/90]_{4s}$ composite for the incident plane at 0° orientation. An ultrasonic pulse with center frequency 2 MHz was used. The thickness of the sample was 2.5 mm, the lamina thickness was 0.156 mm and density was 1.6 g/cm^3. The results of time-delay measurements are shown by dots in Fig. 8. The reconstructed lamina properties are $C_{11} = 121.5$, $C_{22} = 12.1$, $C_{12} = 4.19$, $C_{23} = 8.45$, $C_{55} = 9.27$ (unit: GPa). The computed time delay using these properties is shown in Fig. 8 by solid lines.

4.3. Effective property determination using dynamic Floquet wave homogenization

After lamina properties are measured we can determine the effective dynamic elastic properties of the multidirectional composite. At low frequencies we homogenize the composite using a Floquet wave method

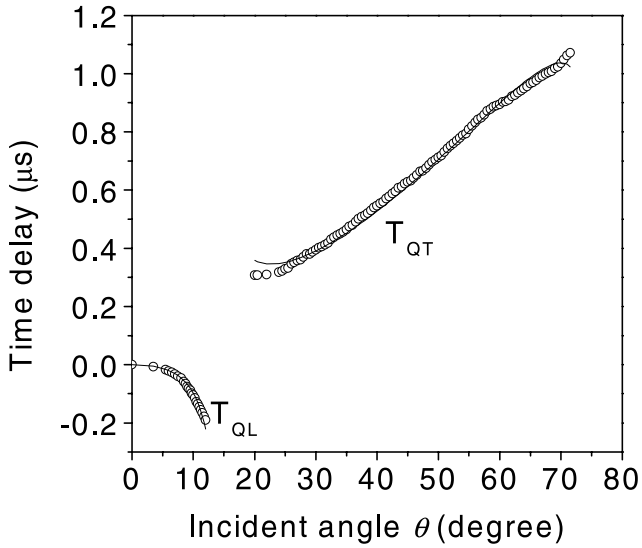

Fig. 8. Comparison of the experimental time delay (◯) and that calculated using reconstructed set of data (—) for $[0/90]_{4s}$ composite. Incident plane is at $\alpha = 0°$.

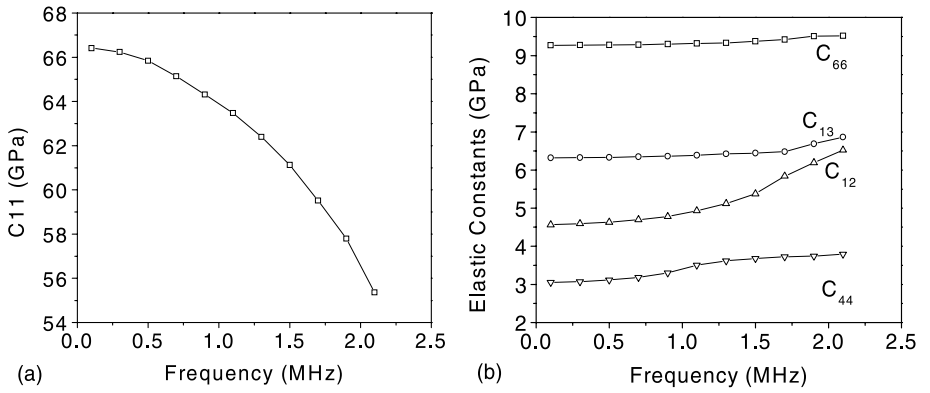

Fig. 9. Frequency dependent effective elastic constants of the $[0/90]_{4s}$ composite calculated using dynamic homogenization method: (a) C_{11} and (b) C_{12}, C_{13}, C_{44}, C_{66}.

transforming the composite to a dispersive homogeneous anisotropic medium. One can see from the Floquet wave spectrum (Fig. 5b) that in the homogenization zone which is at frequencies below the first stop band, the Floquet wave behavior in the periodic medium is equivalent to that of a plane wave in the effective anisotropic medium (three waves may propagate and their critical angles exist). At a given frequency, we calculate the slowness surface for Floquet waves and match it to the slowness surface for bulk waves in homogenized anisotropic media (Wang and Rokhlin, 2000). The Floquet slowness surface is calculated by Eq. (9) using the known composite layout and lamina properties. The match is performed using least-squares minimization searching for the unknown effective elastic constants which are determined uniquely from the plane wave slowness surface. Fig. 9 shows the effective elastic constants as functions of frequency computed for the above lamina elastic properties.

5. Conclusions

Commonly used multidirectional graphite/epoxy composites are extremely nonhomogeneous and anisotropic. These together with structural periodicity lead to very complicated transitivity spectra in frequency and angle domains. When the incident angle deviates from normal incidence on composite structures the transmitted signals are strongly distorted and their peak amplitude declines sharply. However at incident angle about 50° in a fluid a transmission window exists at frequencies below 2 MHz. This makes it possible to use obliquely incident waves for composite evaluation. The Floquet wave theory has been applied to determination of the elastic constants of a single ply from time-delay measurement of obliquely through transmitted ultrasonic waves in multidirectional composites. Reconstruction of the lamina elastic constants from measured time-delay data has been done by nonlinear least-squares minimization. It was also shown that the ply elastic properties can be measured using time-resolved line focus acoustic microscopy.

References

Achenbach, J.D., 1974. Wave propagation in fiber reinforced composites. In: Sendeckyi, G.P. (Ed.), Composite Materials: Mechanics of Composite Materials, vol. 2. Academy Press, New York, London (Chapter 8).

Achenbach, J.D., Sun, C.T., Herrmann, G., 1968. On the vibrations of a laminated body. J. Appl. Mech. 35, 689–696.

Adler, E.L., 1990. Matrix methods applied to acoustic waves in multilayers. IEEE Trans. Ultrason. Ferroelec. Freq. Contr. 37, 485–490.

Braga, A.M., Herrmann, G., 1992. Floquet waves in anisotropic periodically layered composites. J. Acoust. Soc. Am. 91, 1211–1227.

Briggs, G.D., 1992. Acoustic Microscopy. Clarendon Press, Oxford.

Castaings, M., Hosten, B., 1993. Transfer matrix of multilayered absorbing and anisotropic media. Measurements and simulations of ultrasonic wave propagation through composite materials. J. Acoust. Soc. Am. 94, 1488–1495.

Cheng, A., Murray, T.W., Achenbach, J.D., 2001. Simulation of laser-generated ultrasonic waves in layered plates. J. Acoust. Soc. Am. 110 (2), 848–855.

Chimenti, D.E., 1997. Guided waves in plates and their use in materials characterization. Appl. Mech. Rev. 50, 247–284.

Chimenti, D.E., Nayfeh, A.H., 1990. Ultrasonic reflection and guided wave propagation in biaxially laminated composite plates. J. Acoust. Soc. Am. 87 (4), 1409–1415.

Chu, Y.C., Rokhlin, S.I., 1994. A method for determination of elastic constants of a unidirectional lamina from ultrasonic bulk velocity measurements on [0/90] cross-ply composites. J. Acoust. Soc.Am. 96, 342–354.

Datta, S.K., 2000. In: Chou, T.W. (Ed.), Comprehensive Composite Materials, vol. 1. Elsevier, Amsterdam, pp. 511–558 (Chapter 1.18).

Fahmy, A.H., Adler, E.L., 1973. Propagation of acoustic waves in multilayers: a matrix description. Appl. Phys. Lett. 20, 495–497.

Fryer, G.J., Frazer, L.N., 1984. Seismic waves in stratified anisotropic media. Geophys. J. R. Astron. Soc. 78, 691–710.

Fryer, G.J., Frazer, L.N., 1987. Seismic waves in stratified anisotropic media II. Elastodynamic eigensolutions for some anisotropic systems. Geophys. J. R. Astron. Soc. 91, 73–101.

Green, E.R., Green, W.A., 2000a. Transient response of quasi-isotropic fiber composite laminates to internal line sources. J. Acoust. Soc. Am. 108 (5), 1989–1997.

Green, E.R., Green, W.A., 2000b. A computational method for wave propagation from a point load in an anisotropic material. Ultrasonics 38, 262–266.

Guo, Z., Achenbach, J.D., Madan, A., Martin, K., Graham, M.E., 2000. Integration of modeling and acoustic microscopy measurements for thin films. J. Acoust. Soc. Am. 107 (5), 2462–2471.

Hosten, B., 1992. Stiffness matrix invariants to validate the characterization of composite materials with ultrasonic methods. Ultrasonics 30, 365–371.

Hosten, B., Castaings, M., 1993. Delta operator technique to improve the Thomson–Haskell method stability for propagation in multilayered anisotropic absorbing plates. J. Acoust. Soc. Am. 95, 1931–1941.

Kausel, E., 1986. Wave propagation in anisotropic layered media. Int. J. Num. Meth. Eng. 23, 1567–1578.

Kausel, E., Roesset, J., 1981. Stiffness matrices for layered soils. Bull. Seism. Soc. Am. 71, 1743–1761.

Kennett, B.L., 1983. Seismic Wave Propagation in Stratified Media. Cambridge University Press, New York.

Kennett, B.L., Kerry, N.J., 1979. Seismic waves in a stratified half space. Geophys. J. R. Astron. Soc. 57, 557–583.

Lee, Y.C., Kim, J.O., Achenbach, J.D., 1994. Measurement of stresses by line-focus acoustic microscopy. Ultrasonics 32, 359–365.

Li, W., Achenbach, J.D., 1996. $V(z)$ measurement of multiple leaky surface wave velocities for elastic constant determination. J. Acoust. Soc. Am. 100, 1529–1537.

Li, W., Achenbach, J.D., 1997. Determination of elastic constants by time-resolved line focus acoustic microscopy. IEEE Ultrason. Ferrelec. Freq. Control 44, 681–687.

Lih, S.S., Mal, A.K., 1996. Response of multilayered composite laminates to dynamic surface loads. Composite Part B 27, 633–641.

Lobkis, O.I., Chimenti, D.E., Zhang, H., 2000. In-plane elastic property characterization in composite plates. J. Acoust. Soc. Am. 107 (4), 1852–1858.

Mal, A.K., 1988. Wave propagation in layered composite laminates under periodic surface loads. Wave Motion 9, 231–238.

Mal, A.K., Ting, T.C.T. (Eds.), 1988. Wave Propagation in Structure Composites. ASME-AMD.

Nayfeh, A.H., 1991. The general problem of elastic wave propagation in multilayered anisotropic media. J. Acoust. Soc. Am. 89, 1521–1531.

Nayfeh, A.H., 1995. Wave Propagation in Layered Anisotropic Media. North-Holland, New York.

Nayfeh, A.H., Chimenti, D.E., 1991. Elastic wave propagation in fluid-loaded multiaxial anisotropic media. J. Acoust. Soc. Am. 89 (2), 542–554.

Postma, G.W., 1955. Wave propagation in a stratified medium. Geophysics 20, 780–806.

Rokhlin, S.I., Huang, W., 1992. Ultrasonic wave interaction with a thin anisotropic layer between two anisotropic solid: II. Second-order asymptotic boundary condition. J. Acoust. Soc. Am. 92 (3), 1729–1742.

Rokhlin, S.I., Bolland, T.K., Adler, L., 1986. Reflection and refraction of elastic waves on a plane interface between two generally anisotropic media. J. Acoust. Soc. Am. 79, 906–918.

Rokhlin, S.I., Wang, W., 1992. Double through-transmission bulk wave method for ultrasonic phase velocity measurement and determination of elastic constants of composite materials. J. Acoust. Soc. Am. 91, 3303–3312.

Rokhlin, S.I., Xie, Q., Liu, Y., Wang, L., 1999. Ultrasonic study of quasi-isotropic composites. In: Thompson, D.O., Chimenti, D.E. (Eds.), Review of Progress in QNDE, vol. 18B. Plenum, New York, pp. 1521–1528.

Rokhlin, S.I., Wang, L., 2002. Stable recursive algorithm for elastic wave propagation in layered anisotropic media: stiffness matrix method, J. Acoust. Soc. Am. 112 (3), Sept.

Rose, W.R., Rokhlin, S.I., Adler, L., 1987. Evaluation of anisotropic properties of graphite–epoxy composite plate using Lamb waves. In: Thompson, D.O., Chimenti, D.E. (Eds.), Review of Progress in QNDE, vol. 6B. Plenum, New York, pp. 1111–1118.

Schmidt, H., Tango, G., 1986. Efficient global matrix appraoch to the computation of synthetic seismograms. Geophys. J. R. Astron. Soc. 84, 331–359.

Schmidt, H., Jensen, F.B., 1985. A full wave solution for propagation in multilayered viscoelastic media with application to Gaussian beam reflection at fluid–solid interfaces. J. Acoust. Soc.Am. 77, 813–825.

Schoenberg, M., Muir, F., 1989. A calculus for finely layered anisotropic media. Geophysics 54, 581–589.

Shah, A.H., Datta, S.K., 1982. Harmonic waves in a periodically laminated medium. Int. J. Solids Struct. 18, 397–410.

Sun, C.T., Achenbach, J.D., Herrmann, G., 1968. Continuum theory for a laminated medium. J. Appl. Mech. 35, 408–411.

Wang, Y., Rajapakse, R.K.N.D., 1994. An exact stiffness method for elastodynamics of a layered orthotropic half-plane. J. Appl. Mech. 61, 339–347.

Wang, L., Rokhlin, S.I., Hsu, N.N., 1998. Time resolved line focus acoustic microscopy of composites. In: Thompson, D.O., Chimenti, D.E. (Eds.), Review of Progress in QNDE, vol. 18B. Plenum, New York, pp. 1321–1328.

Wang, L., Rokhlin, S.I., 2000. Analysis of ultrasonic wave propagation in multiply composites: homogenization and effective anisotropic media. In: Thompson, D.O., Chimenti, D.E. (Eds.), Review of Progress in QNDE, vol. 20B. Plenum, New York, pp. 1015–1022.

Wang, L., Rokhlin, S.I., 2001. Stable reformulation of transfer matrix method for wave propagation in layered anisotropic media. Ultrasonics 39, 407–418.

Wang, L., Rokhlin, S.I., 2002a. Recursive stiffness matrix method for wave propagation in stratified media. Bull. Seism. Soc. Am. 92, 1129–1135.

Wang, L., Rokhlin, S.I., 2002b. Floquet wave homogenization of periodic anisotropic media, J. Acoust. Soc. Am. 112, 38–45.

Wang, L., Rokhlin, S.I., 2002c. Floquet wave ultrasonic method for determination of single ply moduli in multi-directional composites, J. Acoust. Soc. Am. 112 (3), Sept.

Xiang, D., Hsu, N.N., Blessing, G.V., 1996. The design, construction and application of a large aperture line-focus PVDF transducer. Ultrasonics 34, 641–647.